

Comprehensive characterizing of vortex phases in type-II superconductor $\text{YBa}_2\text{Cu}_3\text{O}_{7-x}$ by a magnetoelectric technique

Peipei Lu^{1,2,*}, Jing Zhang^{1,*}, Jun Lu³, Xiaoyuan Zhou⁴, Young Sun^{3,4,†} and Yisheng Chai^{1,4,‡}

¹Low Temperature Physics Laboratory, College of Physics, Chongqing University, Chongqing 401331, China

²College of Physics, Hebei Normal University, Shijiazhuang 050024, Hebei, China

³ Beijing National Laboratory for Condensed Matter Physics, Institute of Physics, Chinese Academy of Sciences, Beijing 100190, China

⁴Center of Quantum Materials and Devices, Chongqing University, Chongqing 401331, China

[†]yschai@cqu.edu.cn

[‡]youngsun@cqu.edu.cn

* P. L. and J. Z. contributed equally to this work

Abstract

The vortex phases in type-II superconductors are very important since they determine many magnetic and electric properties of the parent compound. However, a universal tool to characterize the vortex phases is still lacking. We demonstrate in a type-II superconductors $\text{YBa}_2\text{Cu}_3\text{O}_{7-x}$ polycrystal sample that its vortex phases and phase boundaries can be comprehensively studied by a magnetoelectric technique. In this method, a thin piezoelectric material $0.7\text{Pb}(\text{Mg}_{1/3}\text{Nb}_{2/3})\text{O}_3$ - 0.3PbTiO_3 (PMN-PT) is mechanically bonded with $\text{YBa}_2\text{Cu}_3\text{O}_{7-x}$ to form a laminate structure and act as a strain gauge. The phase diagram of the $\text{YBa}_2\text{Cu}_3\text{O}_{7-x}$ polycrystalline was explored by this method. Surprisingly, it can accurately estimate the H_{c1} , irreversible line, H_{c2} and distinguish among vortex glass, vortex liquid, non-vortex states. Moreover, it can probe the dynamic response under different frequencies and observe the threshold phenomena of vortex liquid phase. It can even account for the density of vortices in the vortex solid phase. Our technique is readily extended to investigate the vortex phases in other type-II superconductors.

I. INTRODUCTION

Superconductors (SC) have two fundamental properties, zero resistivity and perfect diamagnetism which can fully exclude small external magnetic field in principle [1-3]. The $\mu_0 H$ field inside the SC remains zero until the superconductivity is fully destroyed when the external field H is above a critical field H_{c1} in type-I SC. However, due to the negative interface energy between superconducting and normal phases in the type-II SC, the magnetic field larger than H_{c1} can sometime penetrate the SC phase instead of destroying it. Above H_{c1} , the magnetic field enters a type II SC in the form of quantized vortices, each carrying one quantum of vortex $\phi_0 = hc/2e$, and the vortices could form regular triangular or square lattice as a two-dimensional solid state [4]. In an ideal two-dimensional crystal without any impurity/imperfection, the vortices will move under external current to lose zero resistivity [5]. In reality, the impurities in the parent material can pin the vortices so that vortex lattice can keep its position under small current. Upon warming, disorder or high enough current, the lattice phase can melt into liquid phase, leading to finite resistance ($R \neq 0$) under driven electric field [6] and dissipating behaviors (imaginary part of magnetic susceptibility $\chi'' \neq 0$) under driven magnetic field [7]. In liquid phase, the vortex can detach from the pinning center under certain magnitude of external stimulus which is regarded as a threshold behavior [8]. The transition between vortex liquid and solid phases has been confirmed around an irreversible temperature T_{irr} [9]. Due to the quantum nature of the vortex, it can act as a superconducting qubit in quantum computing [10] and host Majorana zero modes for topological quantum computing found by STM/S in the

vortex cores of $\text{FeTe}_{0.55}\text{Se}_{0.45}$ [11]. Moreover, the strong pinning in the vortex solid phase in type-II SC is vitally important in its application, especially for superconducting magnets and a planar magnetic field source [12]. Therefore, identification of the vortex phases and the understanding of their dynamic responses to external stimulus are crucial in its applications.

To identify the vortex phases and study their dynamics, some traditional methods must be combined to have a fully understanding. (1) Direct resistivity measurement can only distinguish the superconducting phase and normal phase, rather than the vortex phases. Therefore, large current density must be introduced to measure the current-voltage relationship around T_c and to find the phase transitions between vortex glass and liquid or normal and liquid phases [13]. (2) dc magnetization (M) can find the T_{irr} by performing the zero-field-cooling (ZFC) and field-cooling (FC) temperature scans [14]. But for larger H , M becomes positive for both FC and ZFC, making it ambiguous to judge the existence of vortex phases. Moreover, in magnetic field scan, the butterfly M - H loop with large hysteresis is a typical character of the vortex solid phase due to strong pinning. (3) The ac susceptibility $\chi = \chi' + i\chi''$ is a sensitive and nondestructive method to measure SC properties [15]. The negative real part χ' indicates the diamagnetism of superconductivity. The imaginary part χ'' reflects the dissipative nature of the vortex liquid phase due to the depinning, while zero value of χ'' at lower temperatures points to a vortex solid phase. However, its real part only measures the superconducting volume instead of the vortex density directly. (4) Magneto-optical [16] or Bitter technique [17] method can directly

observe vortices or their slow dynamics. However, these methods require a high smoothness of the sample surface. Also, they cannot judge the vortex density in the bulk sample directly, nor the fast dynamics due to the speed limit in imaging. (5) Neutron scattering experiments can be performed to determine the structure of the vortex lattice and its melting behaviors since the scattering pattern directly reveals the reciprocal lattice [18-20]. The diffraction signal disappears when the sample is in the normal state. However, this method requires a long time to collect enough data and is unable to probe the dynamic behaviors of the vortex liquid phase. (6) Magnetostriction method can also be used to detect the property of the vortex phases [21]. Usually, there is a large magnetostriction in the vortex phases due to the pinning force acting on the vortices. However, due to the slow measurement speed, dynamic behaviors in the liquid phase have rarely been studied. Therefore, one method that is relatively simple, cheap and fast, which is able to characterize the vortex phases and phase boundaries comprehensively, is still lacking.

Recently, a new method probing the magnetic skyrmion system, including the mixed and solid phases, is invented by using a composite magnetoelectric (ME) technique [22, 23]. In our measurements, a piezoelectric phase is mechanically bonded with a magnetostrictive phase to form a laminate structure, as schematically shown in Figure 1(a). The magnetostriction $\lambda = \Delta L/L$ of magnetic phase can be converted into an electrical signal via interfacial strain coupling, as shown in Figure 1(b). When an ac magnetic field H_{ac3} is applied, an out-of-plane ac voltage V_{ac3} signal can be induced in the piezoelectric phase with thickness t and the longitudinal ME

voltage coefficient $\alpha_{E33}(=V_{ac3}/tH_{ac3})$ for in-plane isotropic magnetostrictions in the piezoelectric material is given by [22-24]:

$$\alpha_{33} = \frac{V_{ac3}}{tH_{ac3}} \propto k d_{31} q_{13} \quad (1)$$

where k ($0 < k < 1$) is interface coupling parameter, d_{ij} defines the transverse piezoelectric coefficient and $d_{31}=d_{32}$ for polycrystalline sample and $q_{13} = d\lambda_1/dH_3$. As for the MnSi single crystal sample, we are able to find the existence of skyrmion solid phase surrounded by mixed phases with this technique. The similar two-dimensional particle system—the vortex phases in the type-II SC, usually have strong magnetostrictive behavior [21]. Therefore, this technique can be applicable to the study of the vortex phases in the type-II SC.

In this work, a cheap and simple composite ME technique has been introduced to comprehensively study the vortex phases in type-II High T_c superconductor $\text{YBa}_2\text{Cu}_3\text{O}_{7-x}$ (YBCO) polycrystal. We demonstrate that this method can comprehensively investigate and plot the vortex phase diagram, including the H_{c1} , irreversible line, H_{c2} and distinguish among the vortex glass, vortex liquid, non-vortex states. Moreover, it can probe the dynamic response of vortex liquid phase under different frequencies and stimulus strengths. Most important, it can quantitatively measure the density of vortex in the vortex solid phase.

II. EXPERIMENTAL

Commercial YBCO polycrystalline samples are bought from Central Iron & Steel Research Institute, China. They are grown by melt-textured method with very

strong pinning forces to the vortices. A standard four-probe method is applied in the resistance measurements. To reduce the contact resistance, the YBCO polycrystal was annealed in air at 425 °C for 6 hours before measurement. Magnetization was measured by the VSM option of Physical Property Measurement System (PPMS, Quantum Design, Dynacool). The ac susceptibility χ of YBCO were measured by ACMS option of PPMS with various frequencies under $H_{ac} = 5$ Oe.

The composite ME structure is prepared by bonding a YBCO polycrystalline sample to a piezoelectric material $0.7\text{Pb}(\text{Mg}_{1/3}\text{Nb}_{2/3})\text{O}_3\text{--}0.3\text{PbTiO}_3$ (PMN-PT) [001]-cut single crystal ($t = 0.2$ mm) with silver epoxy (Epo-Tek H20E, Epoxy Technology Inc.). Before any electrical measurement, the PMN-PT is pre-poled along the thickness direction by a poling electric field of 5.5 kV/cm for 1 hour at room temperature. An ac magnetic field H_{ac} is applied by a coil and the generated ac ME voltage $V_{ac} (=V_x+iV_y)$ on the YBCO/PMN-PT is measured by a lock-in amplifier (NF Corporation LI5645) with a commercial sample stick (MultiField Tech.), as shown in [Figure 1\(c\)](#). The ac ME voltage coefficient $\alpha = V_{ac}/tH_{ac} = \alpha_x+i\alpha_y$ is calculated. The temperature and dc magnetic field conditions are provided by PPMS.

III. RESULTS AND DISCUSSIONS

The superconductivity of YBCO sample was first characterized by the conventional resistance and dc magnetization. The resistance of YBCO as a function of temperature $R(T)$ under different dc magnetic fields is measured, as shown in [Figure 2\(a\)](#). The characteristic temperatures of T_{on} and T_{end} can be defined where the

resistance starts to decrease and becomes zero, respectively. Above T_{on} , YBCO is in the normal state while below T_{end} , it is in the vortex glass phase due to strong pinning and polycrystalline nature of the specimen. In between, it is expected to be in the vortex liquid phase. At zero field, the T_{on} and T_{end} are clearly observed ≈ 91 K and 83 K, respectively. With the increase of the external magnetic field, the transition temperatures are suppressed continuously with slight broadening. Note that, there are two steps between T_{on} and T_{end} in $R(T)$ curves, showing the inhomogeneity in our YBCO sample.

The temperature dependent magnetization $M(T)$ in the FC and ZFC processes under 5 mT were performed, as shown in Figure 2(b). Clear diamagnetism is observed below $T_M \approx 89$ K and the superconducting volume fraction is estimated to be 48.4% at 60 K from the ZFC data. Moreover, T_M at this field stands for the irreversible line where the FC and ZFC curves began to merge. Figure 2(c) shows the $M(T)$ curves under various dc magnetic fields for the FC process. The T_M shifts to the lower temperatures with the increase of dc magnetic field. The H - T phase diagram of YBCO sample is plotted, as shown in Figure 2(d). In this sample, T_{on} and T_M are very close which is counterintuitive since the irreversible line and H_{c2} ($<T_{\text{on}}$) line are usually well separated in the high T_c cuprates. Therefore, from the above measurements and the derived phase diagram, it is very hard to pin down those lines separating the vortex solid, liquid, and normal states.

To verify that our composite ME technique is capable of probing the vortex phases in YBCO polycrystal sample, we prepared a ME laminate of YBCO/PMN-PT

plate in composite configuration. The large ME voltage coefficients α of the YBCO/PMN-PT laminate below T_c are indeed observed under finite dc magnetic fields and 1 Oe H_{ac} with a frequency of 199 Hz, as shown in [Figure 3](#). The real part α_x and imaginary part α_y of α at 0 T (without vortex, not shown here) are featureless while passing through T_c so that we treated them as background signals and were subtracted from other data under finite magnetic fields. At 0.1 T for ZFC and FC processes, α_x values separate with each other at low temperature and the FC data is always larger than that of ZFC data, consistent with that of M in [Figure 2\(b\)](#). At T_{irr} , two curves merge, coinciding with the definition of the so-called irreversible temperature. With further increasing temperature, they drastically decrease in two-step way and finally become zero below T_M and T_{on} . In contrast, at low temperature below T_{irr} , the values of α_y are negligibly small for both cases. Above T_{irr} , α_y of ZFC and FC have nearly identical temperature profiles with two peaks centered at $T_{p1} = 84.1$ K and $T_{p2} = 86.7$ K below T_M , which are consistent with the fast drop two-step feature in α_x . Those two steps/peaks features also point to the two-step feature in resistance and indicate two transition temperatures for this sample. The temperature where α_y starts to become zero is defined as T_{ini} , which is lower than T_M and T_{on} .

Nonzero α_x values below T_M and T_{on} strongly indicate the vortex phases while the nonzero α_y values between T_{irr} and T_{ini} point to a dissipative behavior in the superconducting state, like that of ac magnetic susceptibility [\[7\]](#). The similarity between two methods will be compared below in [Figure 4](#). The appearance of peaks

in α_y strongly indicates the vortex liquid phase in type-II SC, and the initial temperature T_{ini} corresponds to the disappearance of vortex phase. Below T_{irr} , the negligible values in α_y and the separation of ZFC and FC signals in α_x are consistent with a vortex glass phase. The smaller α_x in ZFC seems to indicate a smaller vortex density, implying that the magnitude of α_x can be related to the density of vortex. The fact that α_x signal only contains background signal when vortex density is zero without magnetic field, also supports such assumption.

Therefore, to test the above relationship, α_x and α_y under different dc magnetic fields in the FC process of 0.01, 0.02, 0.05, 0.1, 0.2, 0.5, 1, 2, 5 and 9 T are measured, as shown in [Figure 3\(c\)](#) and [3\(d\)](#). With increasing the magnetic field, the magnitude of α_x increases. Moreover, the T_{irr} is suppressed continuously, indicating the bending of irreversible line under high field. In α_y curves, there is a negligible ME signal below the temperature of T_{irr} under every dc magnetic field, proving the existence of the vortex glass phase below this temperature. The values of α_x at 60 K are almost linearly proportional to the dc magnetic field, as shown in the inset of [Figure 3\(c\)](#). Usually, the dc magnetic field is proportional to the density of vortex in vortex solid phase during FC process, verifying that α_x and vortex glass density are linearly correlated. The relationship is different from magnetization and ac magnetic susceptibility measurements that lower vortex density leads to stronger diamagnetic signals [\[7, 14\]](#).

In α_y curves, T_{p1} , T_{p2} and T_{ini} are suppressed to lower temperatures with wider intervals in higher field, implying a vortex liquid phase been pushed to the lower

temperatures. To prove that the non-zero features in α_y correspond to a vortex liquid phase, we directly compared the ac susceptibility and the ac ME voltage coefficient α at 2 T at selected frequencies, as shown in Figure 4. For the real part, χ' (Figure 4(a)) and α_x (Figure 4(c)) become zero at same temperature T_{irr} , while the two-step feature is clearer in α_x than that in χ' . For the imaginary part, χ'' (Figure 4(b)) and α_y (Figure 4(d)) also become zero at same temperature T_{ini} and show three-peak and two-peak features, respectively. The two higher peaks have almost identical temperatures in both tools while the lower T_{p3} can only be observed in χ'' . All three peaks shift to higher temperature with the increase of frequency, as shown in Figure 4(b) and 4(d). The activation energy E_a and characteristic relaxation time τ_0 are fitted by Arrhenius equation for every peak, as shown in Figure 4(e) [25].

$$\ln f = \ln \frac{1}{\tau_0} - \frac{E_a}{RT} \quad (2)$$

Where R is gas constant. The calculated E_a activation energies from the slopes for T_{p1} and T_{p2} by ME voltage (20.8 and 25 meV) and ac susceptibility (22.9 and 32.3 meV) are consistent with each other. The appearance of the third peak in χ'' may be due to the stronger excitation field of 5 Oe. The strong similarity between the imaginary parts of two methods demonstrates the vortex liquid phase between T_{irr} and T_{ini} .

To further reveal the correlation between the vortex density and the real part of ME signal α_x , M and α as a function of magnetic field after ZFC process at 10 and 5 K were measured, respectively, as shown in Figure 5. The quasi-linear diamagnetic feature is clearly observed in $M(H)$ curve below the critical field H_{c1} . Above H_{c1} up to 9 T, the magnitude of M decreases with increasing H , indicating the fast enhancement

of vortex density in the vortex glass phase. As the magnetic field starts to down sweep from 9 T, it induces a fast sign reversal of M which seems to indicate a decrease in the vertex density. Then, from 8 T to -9 T, the M peaks at around zero H , marking a change of vortex density to zero and back to high density again. The entire $M(H)$ loop shows strong hysteresis due to demagnetization effect. In contrast, α_x almost linearly increases or decreases with H and shows very weak hysteresis behaviors while α_y is negligible in the field range studied, as shown in Figure 5(b). In the low field region after ZFC process, the α_x slightly bends up with a larger slope after H_{c1} , as shown in Figure 5(c). This is consistent with the fact that the vortex density enhances faster after this critical field. However, our data indicate different vortex dynamics in the vortex glass phase. 1) The linear and nonzero α_x below H_{c1} indicates that the magnetic vortex lines keep entering the sample in the unideal Meissner state. 2) When H is down swept from 9 T initially, α_x (the vortex density) still slightly increases, instead of drastically decrease as hinted by $M(H)$ curve. 3) As the magnetic field is swept up or down, the vortex density seems to follow that trend without much hysteresis, as indicated by the weak hysteresis in $\alpha_x(H)$ curve. Therefore, the α_x seems to be able to reveal more direct changes in terms of the vortex density in the type-II SC YBCO.

Finally, we sum up all the T scan data to develop a phase diagram of YBCO polycrystal in Figure 6(a). By comparing the characteristic temperatures among different techniques, four phases are identified as: vortex glass, vortex liquid, cluster and normal states. The T_{irr} and T_{end} define the irreversible line separating the vortex glass and vortex liquid phases. T_{ini} defines the transition temperature between vortex

liquid phase and cluster state where SC cluster phase coexists with normal phase without vortex and can be effectively regarded as H_{c2} line. T_M and T_{on} define the transition temperature between cluster and normal states, instead of irreversible line or H_{c2} line, probably due to the inhomogeneity of the sample. To further verify such phase diagram, we varied the magnitude of driven H_{ac} and measured the corresponding ME voltage $V_{ac} = V_x + iV_y$ at 70, 77.5, 81, and 90 K under 2 T, as shown in Figure 6(b) and 6(c). In the normal state (at 90 K), the V_x and V_y are observed almost zero under different H_{ac} . In the vortex liquid phase (at 81 K), the V_y deviates from zero value and quickly increases while V_x quickly deviates from linear behavior under very small $H_{ac} \approx 0.1$ Oe, indicating a very weak threshold behavior due to the liquid nature. Just inside the glass phase (at 77.5 K), the threshold value of H_{ac} becomes about 1 Oe, indicating a stronger pinning of vortex from impurities. When the sample is deep inside the vortex glass phase (at 70 K), the threshold value of H_{ac} is larger than 2 Oe and the V_x has a pure linear behavior with H . Therefore, our ME technique can draw the vortex related phase diagram reliably with clearer characteristics than other conventional methods.

Need to point out that the direct relationship between α_x ($\propto \Delta L/L \Delta H$) and the density of vortex is counterintuitive. Usually, the number of vortices in a SC should be proportional to the change of sample geometry that the $\Delta L/L$ should have a linear relationship with the density of vortex. Then an almost constant α_x would be expected, which is not the case at all. A possible explanation would be that the ac driven field can induce a low frequency eddy current which will drive the vortex ensemble in the

sample and give rise to a torsional deformation of the ME composite. Such deformation would be proportional to the density of the vortex.

Last but not least, we would like to summarize some technical advantages of this method. (1) The accuracy is high and the noise level is low due to the lock-in technique. The smallest resolution of the ME voltage is about $\pm 0.1 \mu\text{V}$, as shown in [Figure 3\(b\)](#) and this sensitivity is limited by the lock-in amplifier. (2) The cost of the measurement is low. The PMN-PT plate is cheap and easy to purchase. The measurement setup is also cheap since we only need extra lock-in amplifier + current source. (3) The sample preparation process is fast and simple. The sample only needs to be bonded with the PMN-PT plate with short pre-poling time (~ 2 h). (4) The measurement speed is 1s/point and is much faster than that of ac susceptibility without a complicated compensation process. (5) The test frequency range is much wider than that of ac susceptibility, *i.e.*, from 1 Hz to 100 kHz.

IV. CONCLUSION

In this work, a new ME technique based on YBCO/PMN-PT structure was successfully fabricated to measure the vortex phases in type-II superconductor YBCO polycrystalline. From the characteristic temperatures found in ME signals, the vortex glass, vortex liquid and non-vortex states are identified with the determination of H_{c1} , irreversible and H_{c2} lines. Moreover, it can probe the dynamic response of vortex liquid phase under different frequencies and stimulus strengths. Most important, quantitative relationship between the real part of ME signal α_x and the vortex density

is revealed. This composite magnetoelectric technique paves a promising avenue in terms of vortex dynamics in all the type-II superconductors.

ACKNOWLEDGEMENTS

This work was supported by the National Natural Science Foundation of China (Grant Nos. 11974065, 52101221), and the National Key Research and Development Program of China (Grant No. 2016YFA0300700), Chongqing Research Program of Basic Research and Frontier Technology, China (Grant No. cstc2020jcyj-msxmX0263), Fundamental Research Funds for the Central Universities, China (2020CDJQY-A056, 2020CDJ-LHZZ-010, 2020CDJQY-Z006), the Natural Science Foundation of Hebei Province (Grant No. A2021205022), Science and Technology Project of Hebei Education Department (QN2021088), Hebei Normal University (Grant No. L2021B09). Y. S. Chai would like to thank the support from Beijing National Laboratory for Condensed Matter Physics. We would like to thank Miss G. W. Wang at Analytical and Testing Center of Chongqing University for her assistance.

References

1. H. K. Onnes, Commun. Phys. Lab. Univ., Leiden, 122 (1911).
2. H. K. Onnes and W. Tuyn, Commun. Leiden Suppl., 50a (1924).
3. W. Meissner and R. Ochsenfeld, Naturwissenschaften, **21**, 787 (1933).
4. G. Blatter, M. V. Feigel'Man, and V. B. Geshkenbein, Rev. Mod. Phys., **66**, 1125 (1994).
5. H. K. Onnes, Commun. Phys. Lab. Univ. Leiden, Suppl., 34 (1913).
6. J. A. Fendrich, W. K. Kwok, J. Giapintzakis, C. J. van der Beck, V. M. Vinokur, S. Fleshier, U. Welp, H. K. Viswanathan, and G. W. Crabtree, Phys. Rev. Lett., **74**, 7 (1995).
7. A. Crisan, Y. Tanaka, D. D. Shivagan, A. Iyo, L. Cosereanu, K. Tokiwa, and T. Watanabe, Jpn. J. Appl. Phys., **46**, L451 (2007).
8. C. Reichhardt and C. J. Olson Reichhardt, Rep. Prog. Phys., **80**, 026501 (2017).
9. P. Chaddah, Pramana-J. Phys., **36**, 353 (1991).
10. M. Kjaergaard, M. E. Schwartz, J. Braumüller, P. Krantz, Joel I.-J. Wang, S. Gustavsson, and W. D. Oliver, Annu. Rev. Condens. Matter Phys., **11**, 369 (2020).
11. S. D. Sarma, M. Freedman and C. Nayak, npj Quantum Information, **1**, 15001 (2015).
12. J. H. Lacy, A. Cridland, J. Pinder, A. Uribe, R. Willetts, and J. Verdu, IEEE Transactions on Applied Superconductivity, **30**, 8 (2020).
13. Y. Liu, Y. S. Chai, H. J Kim, G. R. Stewart, and K. H. Kim, J. Korean Phys. Soc,

- 55**, 383 (2009).
14. A. Galluzzi, A. Nigro, R. Fittipaldi, A. Guarino, S. Pace, and M. Polichetti, J. Magn. Magn. Mater., **475**, 125 (2019).
 15. K. H. Muller, Physica C, **159**, 717 (1989).
 16. P. E. Goa, H. Hauglin, M. Baziljevich, E. Il'yashenko, P. L. Gammel and T. H. Johansen, Supercond. Sci. Technol., **14**, 729 (2001).
 17. S. Ohshima, T. Kawai, S. Kanno, and H. Yamada, Physica C, **372-376**, 1872 (2002).
 18. N. Rosov, J. W. Lynn, and T. E. Grigereita, J. Appl. Phys., **76**, 15 (1994).
 19. M. R. Eskildsen, L. Ya. Vinnikov, T. D. Blasius, I. S. Veshchunov, T. M. Artemova, J. M. Densmore, C. D. Dewhurst, N. Ni, A. Kreyssig, S. L. Bud'ko, P. C. Canfield, and A. I. Goldman, Phys. Rev. B, **79**, 100501R (2009).
 20. J. M. Densmore, P. Das, K. Rovira, T. D. Blasius, L. DeBeer-Schmitt, N. Jenkins, D. McK. Paul, C. D. Dewhurst, S. L. Bud'ko, P. C. Canfield, and M. R. Eskildsen, Phys. Rev. B, **79**, 174522 (2009).
 21. A. Nabialek, H. Szymczak, and V. V. Chabanenko, J. Low Temp. Phys., **139**, 309 (2005).
 22. M. I. Bichurin and V. M. Petrov, Phys. Rev. B, **68**, 054402 (2003).
 23. G. Srinivasan, Annu. Rev. Mater. Res., **40**, 153 (2010).
 24. D. Patil, June-Hee Kim, Y. S. Chai, Joong-Hee Nam, J. H. Cho, B. I. Kim and K. H. Kim, Appl. Phys. Express, **4**, 073001 (2011).
 25. H. Salamati and P. Kameli, J. Magn. Magn. Mater., **278**, 237 (2004).

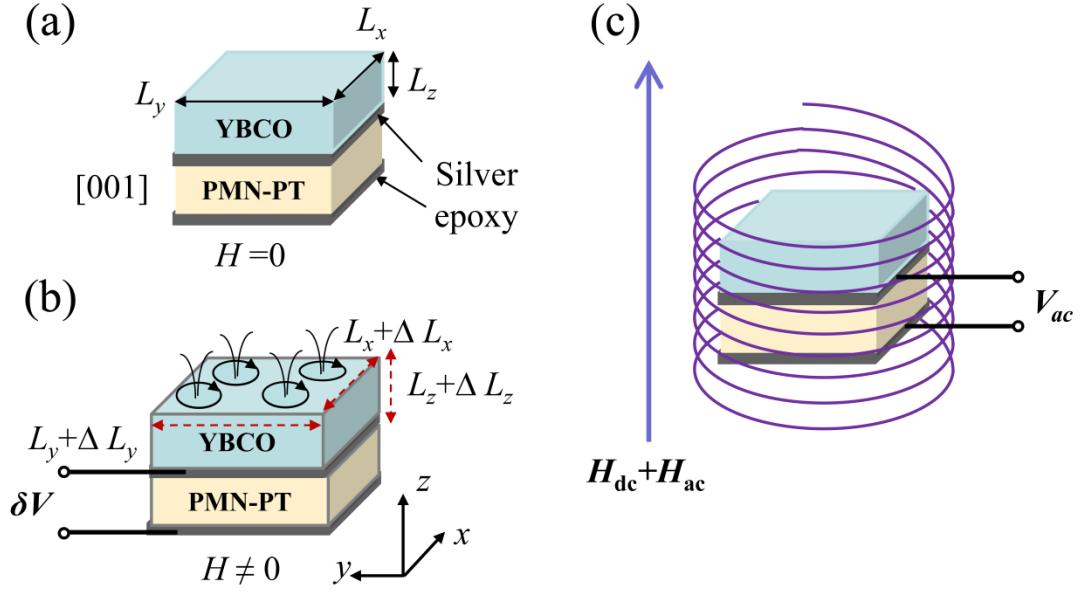


Figure 1. (a) The composite structure of the type-II superconductor polycrystalline YBCO and PMN-PT under zero magnetic field. (b) The shape changes of the YBCO sample in the composite structure under a magnetic field. (c) The magnetoelectric voltage V_{ac} measured under an ac magnetic field by a magnetoelectric technique.

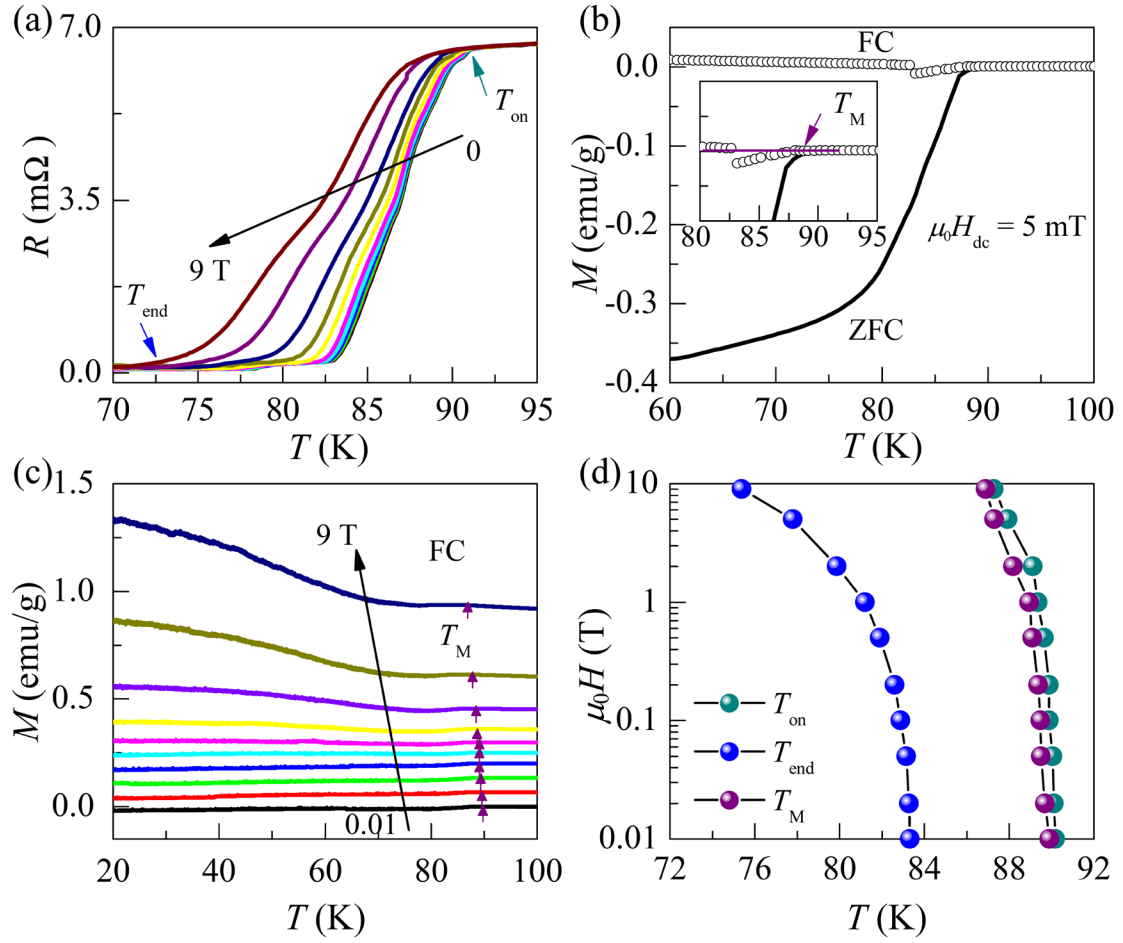


Figure 2. (a) Temperature dependent resistance curves under various magnetic fields of 0, 0.01, 0.02, 0.05, 0.1, 0.2, 0.5, 1, 2, 5 and 9 T for YBCO polycrystalline. (b) Temperature dependence of magnetization under a magnetic field of 5 mT. Both field-cooling (FC) and zero-field-cooling (ZFC) are shown. (c) Temperature dependent magnetization measured in FC condition at 0.01, 0.02, 0.05, 0.1, 0.2, 0.5, 1, 2, 5 and 9 T. (d) The phase diagram of the YBCO polycrystalline according to the data of (a) and (c).

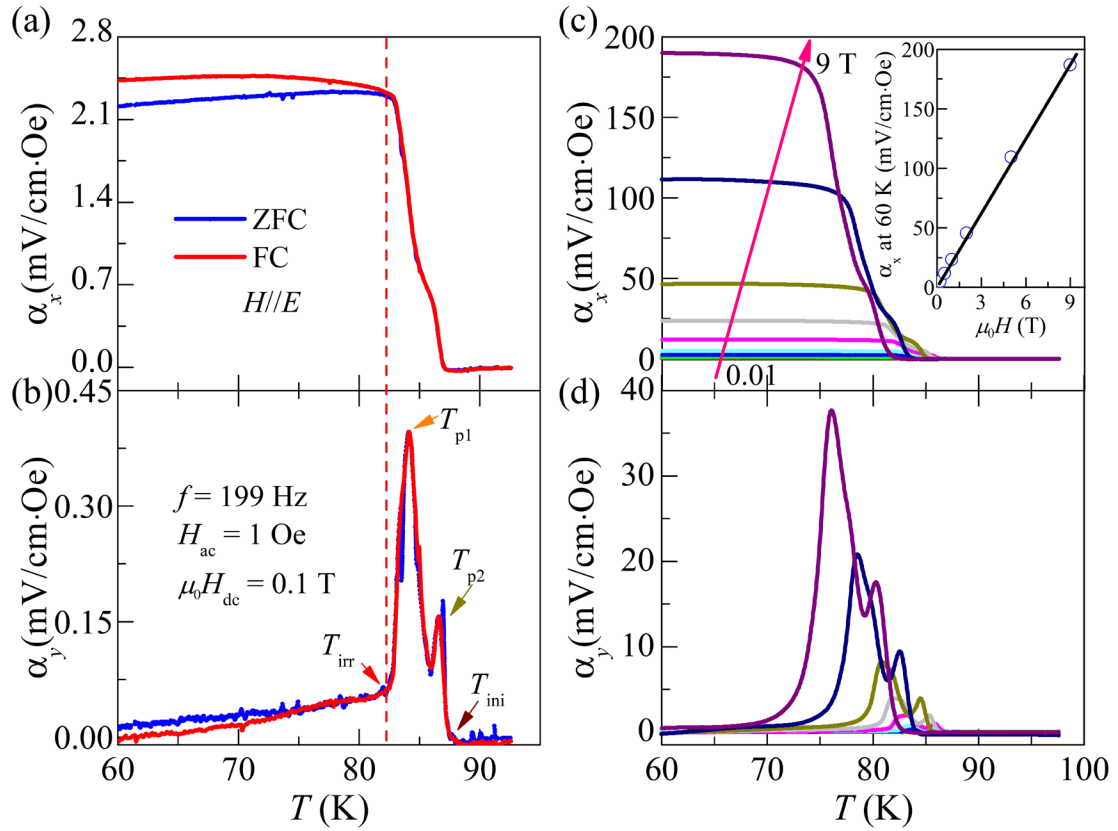


Figure 3. Under an out of plane ac magnetic field of 1 Oe, with a frequency of 199 Hz, the ac ME coefficient α_x (a) and α_y (b) for ZFC and FC processes at 0.1 T. α_x (c) and α_y (d) as a function of temperature for FC process of the YBCO/PMN-PT structure under different magnetic fields of 0.01, 0.02, 0.05, 0.1, 0.2, 0.5, 1, 2, 5 and 9 T.

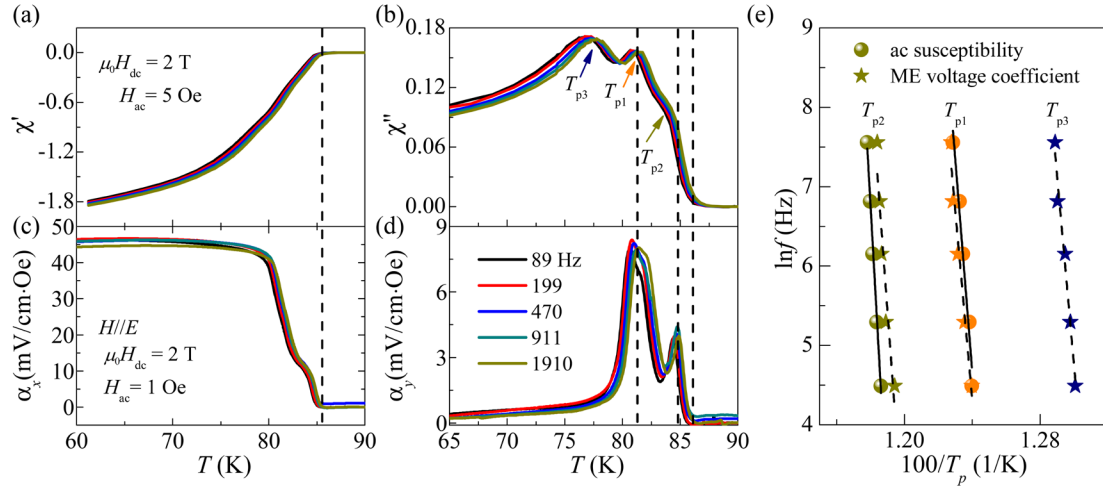


Figure 4. With a dc magnetic field of 2 T and selected frequencies of 89, 199, 470, 997 and 1910 Hz, the ac susceptibility χ' (a) and χ'' (b) under the ac magnetic field of 5 Oe for YBCO polycrystal, the ac ME coefficient α_x (c) and α_y (d) under an ac magnetic field of 1 Oe for YBCO/PMN-PT structure as a function of temperature. (e) The three peak temperatures as a function of frequency in Arrhenius plot.

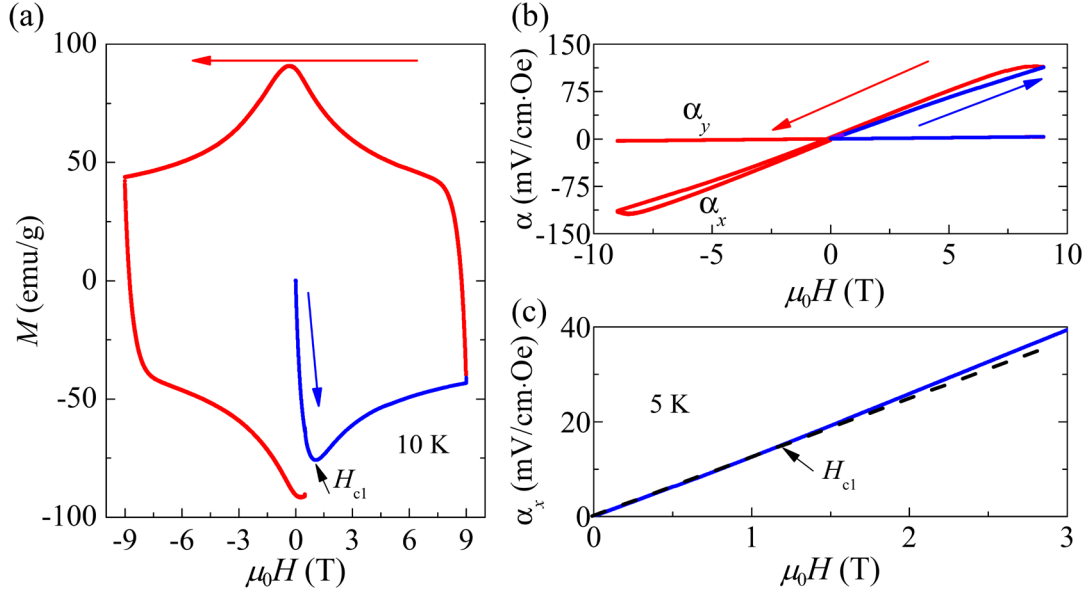


Figure 5. (a) The M - H loop of YBCO polycrystalline. (b) The ac ME coefficient α_x and α_y (b) as a function of magnetic field for YBCO/PMN-PT composite at 5 K. (c) The enlarged view of α_x in (b). α_x deviates from the linear after H_{cl} .

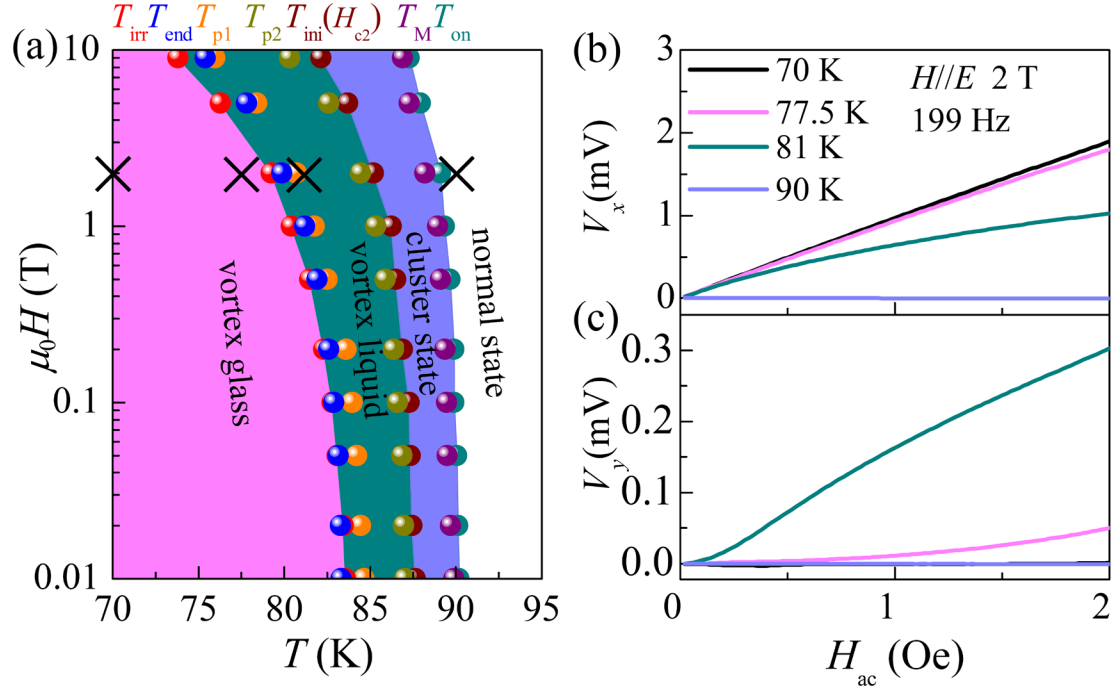


Figure 6. (a) The phase diagram of polycrystalline YBCO from the temperature dependent ME signals of YBCO/PMN-PT structure by magnetoelectric technique. Under a dc magnetic field of 2 T, the ac ME voltage V_x (b) and V_y (c) as a function of H_{ac} at selected temperatures of 70, 77.5, 81 and 90 K.